

This work was written as part of one of the author's official duties as an Employee of the United States Government and is therefore a work of the United States Government. In accordance with 17 U.S.C. 105, no copyright protection is available for such works under U.S. Law.

Public Domain Mark 1.0

<https://creativecommons.org/publicdomain/mark/1.0/>

Access to this work was provided by the University of Maryland, Baltimore County (UMBC) ScholarWorks@UMBC digital repository on the Maryland Shared Open Access (MD-SOAR) platform.

Please provide feedback

Please support the ScholarWorks@UMBC repository by emailing scholarworks-group@umbc.edu and telling us what having access to this work means to you and why it's important to you. Thank you.

Lunar Plasma Environment in Cases with Extreme Solar Wind Conditions:

First Results from 3-D Hybrid Kinetic Modeling and Comparison with ARTEMIS Observations

Alexander S. Lipatov^{a,b}, Menelaos Sarantos^b John F. Cooper^b and Jasper S. Halekas^c

^a Goddard Planetary Heliophysics Institute UMBC, Baltimore MD 21250

^b NASA GSFC, Greenbelt, MD 20771

^c University of Iowa, Iowa City, IA 52242

Fall 2020 AGU Meeting, Dec. 1 - 17, 2020

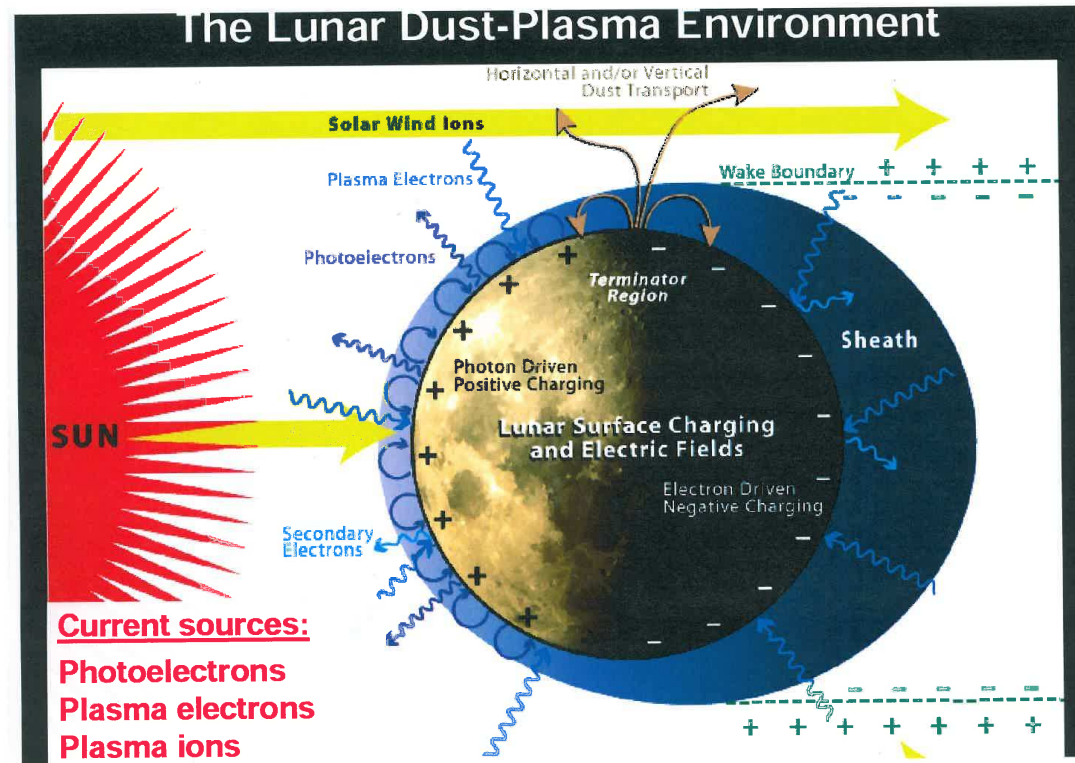
2. Abstract-1

The study of lunar plasma environment's response to the extreme solar wind condition is the main subject of our investigation in this report. The computational model includes the self-consistent dynamics of the light (H_2^+ and He^+), and heavy (Na^+) pickup ions. The electrons are considered as a fluid. The lunar interior is considered as a weakly conducting body. The input parameters are taken from the ARTEMIS observations. The modeling demonstrates a formation of the various plasma structures near the Moon: (a) bow shock wave with split shock transition in case of extreme solar wind density and standard bulk velocity; (b) hyper-sonic/Alfvenic Mach cone in case of extreme solar wind bulk velocity and moderate solar wind density. The modeling shows a strong asymmetry in the solar wind ion VDF which connected with a plasma compression and ion reflection at the bow shock wave/Mach cone front.

3. Motivation and Applications:

- **1. Unique ARTEMIS observations of the solar wind parameters and the lunar plasma environment.**
- **2. Plasma physics of the lunar bow shock-like waves and hypersonic Mach cone.**
- **3. Plasma physics of pickup ions structures and plasma wake.**
- **4. Particle acceleration and electromagnetic perturbations in the lunar plasma environment.**

4. Lunar Surface Plasma Processes. From Stubbs



MAP-PAGE-IMA (Plasma energy Angle and Composition Experiment, and Ion Mass Analyzer) onboard Japanese lunar orbiter **SELENE (KAGUYA)** detected Moon originating ions at 100 km altitude (H^+ , He^{++} , He^+ , C^+ , O^+ , Na^+ , K^+ , and Ar^+)

5. Questions to be answered with hybrid modeling:

- **1. Finite ion gyroradius effects! MHD/Hall MHD/Multifluid MHD cannot produce that!**
- **2. The interpretation of the magnetic field structuring in the plasma wake can allow us to make a conclusion about the composition of the pick ions that were sputtered from the surface of the Moon.**
- **Can the lunar exosphere cause a formation of the bow shock-like waves, whistler/shear Alfvénic waves?**
- **3. What are the plasma processes (particle VDF dynamics, and wave-particle interactions) which occur when the Moon propagates in the solar wind?**

6. Solar Wind - Moon Interaction Models

No pickup ions

- **MHD/C-G-L models** (*zero ion gyroradius/anisotropic pressure*): Wolf, 1968; Spreiter et al., 1970; Catto, 1974
- **Drift-kinetic models** (*drift currents, kinetic approach along the magnetic field*): Whang, 1969; Wang and Ness, 1970; 3-D nonstationary, conducting core - Lipatov, 1974; 1975; 1976
- **Full kinetic/Electrostatic models** (*electron time and spatial scales*): Farrell et al., 1998; Birch and Chapman, 2001
- **Hybrid models** (*finite ion gyroradius effects*): Kallio, 2005; (lunar-like extrasolar planet Lipatov, Motschmann, Bagdonat & Grießmeier, 2005); Travnicek et al., 2005; Wang et al., 2011; Wiehle et al., 2011; Holmström et al., 2012.

Effects of pickup ions

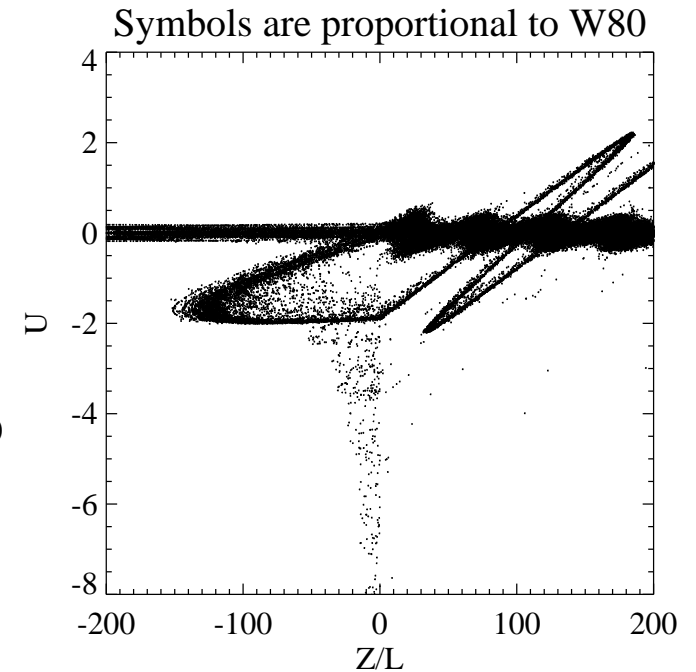
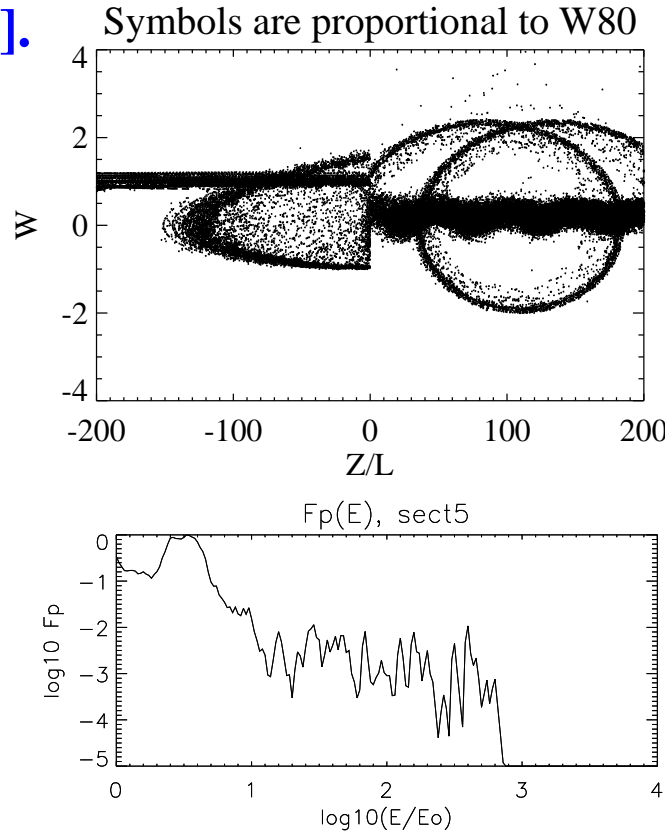
- **Hybrid models** with O^+ , Na^+ and He^+ : Lipatov et al., 2012a; 2012b; 2018.

7. Hybrid Model

- *Kinetic - ions. Fluid - electrons*
- *Interpenetrating flows*
- *Effects of finite ion gyroradius estimated with thermal and bulk velocities: $k_{\perp} \rho_{ci} \geq 1$, $k_{\parallel} \rho_{ci} \geq 1$ and $l \approx \rho_{ci}$; $\omega \approx \Omega_{ci}$*
- *The modeling tool: (a) **Standard PIC** [Harlow, 1957, LANL Report]; **ES - Shape Function Kinetics (SFK)** [Larson & Young, JCP-2015] is a logical extension of **Complex Particle Kinetics (CPK)** [Hewett, JCP-2003; Lipatov, JCP-2012] and **Finite Mass Method (FMM)** [Yserentant et al., AA, NM, SIAM, NM-1996-2007]*
- *The SFK and CPK aim to bridge the gap between continuum and kinetic methods. This method may save a computational resources by factor more than 100 in compare with Standard PIC method*

8. EM-CPK Method for multiple plasma beams [Lipatov,

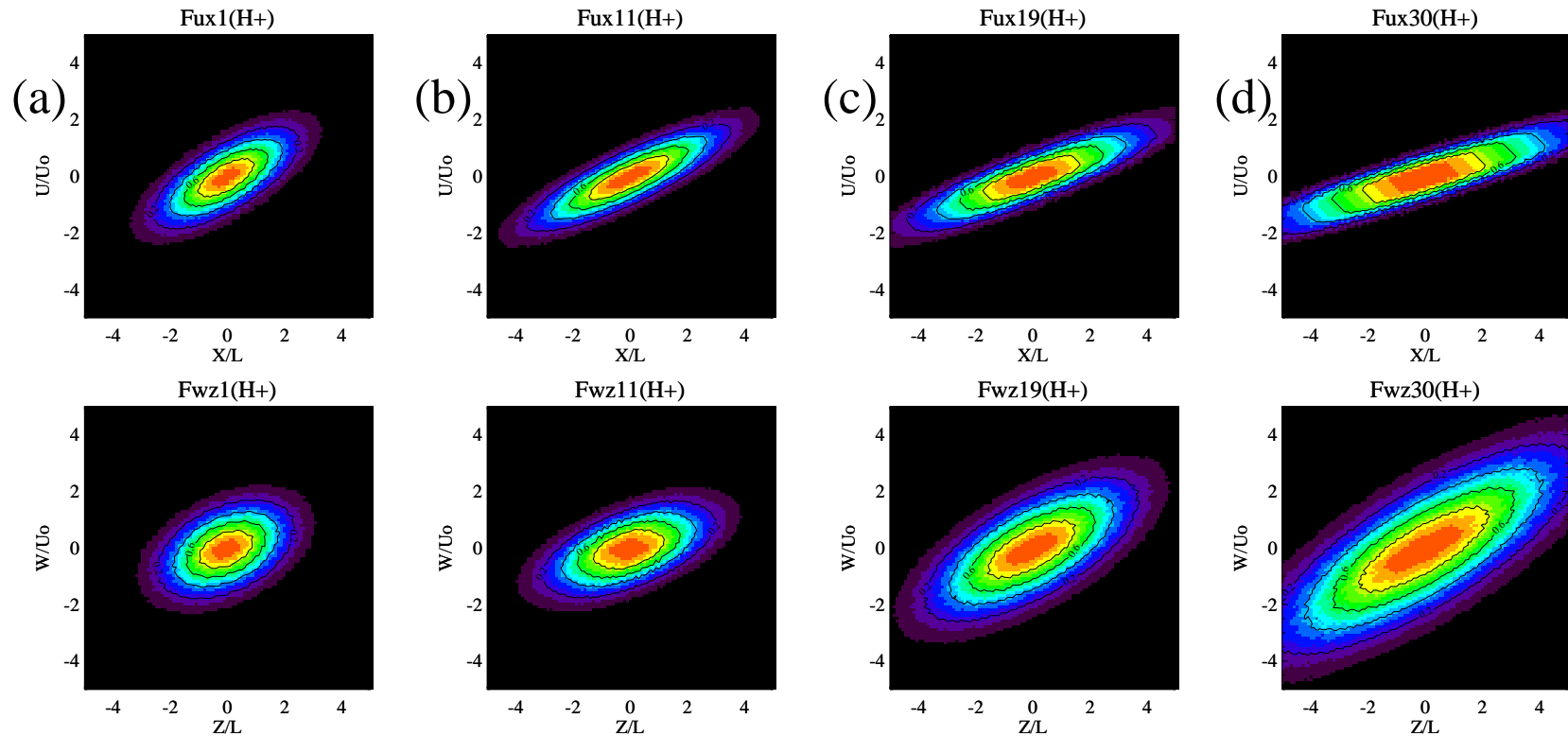
J.Comp.Phys.-2012].



$$f(\mathbf{x}, \mathbf{v}) = \frac{W_{80}}{(2\pi)^3 w_{dox} w_{doy} w_{doz} v_{tox} v_{toy} v_{toz}} \exp \left\{ - \left[\frac{[\mathbf{x} - \mathbf{x}_o - (\mathbf{v} - \mathbf{u}_d)\tau]^2}{2w_{do}^2} + \frac{(\mathbf{v} - \mathbf{u}_d)^2}{2v_{to}^2} \right] \right\}$$

Global time steps: 1) Particle **fragmentation** into the middle and probe particles; 2) Particle **pushing**; 3) Particle **expansion**; 4) Particle **merging**. CPK method produces ion shock surfing acceleration similar to one studied with a standard PIC in Lipatov and Zank [PRL-1999].

9. EM-SFK Method. Individual Macro-Particle \rightarrow 6x6 Matrix [Li-patov et al., GEM-2018].



SFK element dynamics upstream (a and b) and downstream (c and d) of shock front.

Global time-step:

- SFK elements updating **via the point particle dynamics** selected inside the element.
- SFK elements restoring with **covariance matrices**.
- **SFK element cluster reconstruction** via **Expectation-Maximization** algorithm for the **Gaussian Mixture Model in Machine Learning**.

10. Model of Neutral Exosphere and PI Production

3-species description for the neutral exosphere of the exponential form:

$$(1) \quad n_{\text{neutral},k} \approx \Psi(\theta, \phi) n_{\text{exo},k} \exp\left(-\frac{(r - r_{\text{exobase},k})}{h_{\text{exo},k}}\right),$$

where $n_{\text{exo},k}$ denotes the maximum value of the neutral density extrapolated to the surface of the Moon, $r_{\text{exobase},k} = R_{\text{M}} = 1740$ km. Index k **denotes** $\text{Na}, \text{He}, \text{H}_2$.

Ion production from the exosphere:

$$(2) \quad G_{\text{exo},k} \propto \Psi(\theta, \phi) \nu_{i,k} n_{\text{exo},k} \exp\left[-\frac{(r - r_{\text{exobase},k})}{h_{\text{exo},k}}\right].$$

$n_{\text{exo},k}$ denotes the value of neutral component density at $r = r_{\text{exobase}}$ and $\nu_{i,k}$ is the effective ionization rate per atom or molecule of species k . **References:** Hartle & Killen, 2005; Hartle, Sarantos & Sittler, 2011; Wang et al., 2011; Potter & Morgan, 1988; McLain et al., 2011.

11. Initial and Boundary Condition

Initial Condition: SuperAlfvénic and supersonic background plasma flow with a homogeneous spatial distribution and a Maxwellian velocity distribution; Pickup ions have a weak density and spherical spatial distribution.

Boundary Condition. At the side boundaries we use a damping boundary condition for the electromagnetic field. At the downstream boundary we use a **”Sommerfeld” radiation condition for the magnetic field** and a **free escape condition for particles** with re-enter of the portion of particle from outflow plasma. The magnetic field and electric fields are $\mathbf{B} = \mathbf{B}_0$ and $\mathbf{E} = -\mathbf{U}_0 \times \mathbf{B}_0$. We use an **absorption boundary condition** for particles that interact with the surface of the Moon. **Lunar interior** is considered as **weakly conducting body** in these models. The axis \mathbf{X} is directed against from the Sun, \mathbf{Y} axis is directed in the direction of Earth’s orbit, and \mathbf{Z} axis completes the right-handed system.

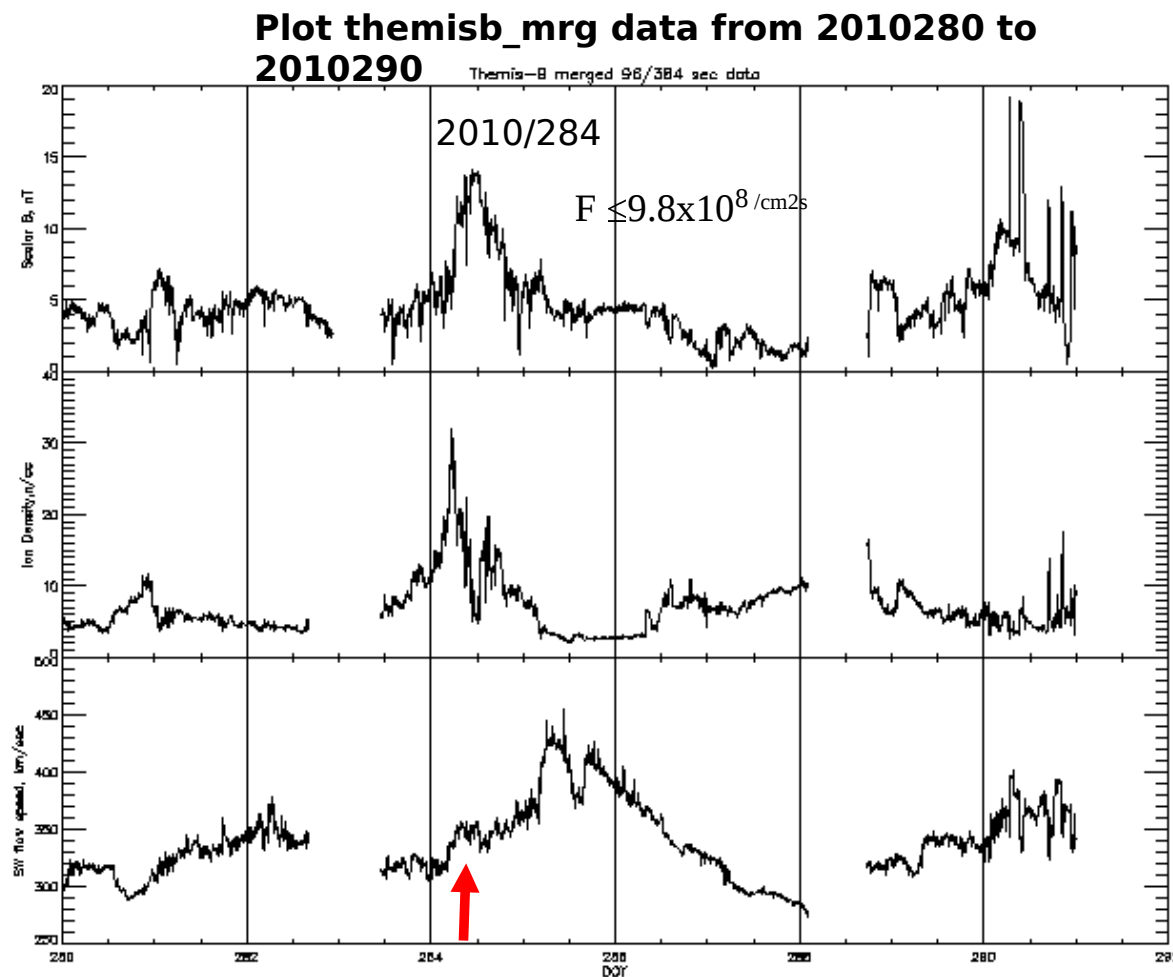
12. Plasma Parameters

Table 1:

Case	SW density	B-field θ_{BU}	Velocity	Production rate of pickup ions	$\frac{T_{\parallel, H^+}}{T_{\perp, H^+}}$ $\delta N^+ / N_0$ at front
1, 90w1CFF	50 cm^{-3}	30 nT 90°	450 km/s	$G_{Na^+} \approx 1.44 \times 10^{22} \text{ s}^{-1}$ $G_{He^+} \approx 1.44 \times 10^{20} \text{ s}^{-1}$ $G_{H_2^+} \approx 7.2 \times 10^{21} \text{ s}^{-1}$	$\approx (0.5 - 0.7)$ ≈ 2.4
2, 90w1CF	50 cm^{-3}	30 nT 90°	450 km/s	$G_{Na^+} \approx 7.2 \times 10^{21} \text{ s}^{-1}$ $G_{He^+} \approx 7.2 \times 10^{19} \text{ s}^{-1}$ $G_{H_2^+} \approx 3.6 \times 10^{21} \text{ s}^{-1}$	$\approx (0.49 - 0.51)$ ≈ 1.75
3, 83w1CF	15 cm^{-3}	16.67 nT 83°	400 km/s	$G_{Na^+} \approx 7.2 \times 10^{21} \text{ s}^{-1}$ $G_{He^+} \approx 7.2 \times 10^{19} \text{ s}^{-1}$ $G_{H_2^+} \approx 3.6 \times 10^{21} \text{ s}^{-1}$	≈ 0.8 ≈ 1.55
4, 90rBB	3 cm^{-3}	5.2 nT 90°	1525 km/s	$G_{Na^+} \approx 5.5 \times 10^{22} \text{ s}^{-1}$ $G_{He^+} \approx 5.5 \times 10^{20} \text{ s}^{-1}$ $G_{H_2^+} \approx 2.86 \times 10^{22} \text{ s}^{-1}$	$\approx (0.88 - 0.95)$ $\approx (2.4 - 2.6)$
5, 90rB	3 cm^{-3}	5.2 nT 90°	1525 km/s	$G_{Na^+} \approx 2.66 \times 10^{22} \text{ s}^{-1}$ $G_{He^+} \approx 2.77 \times 10^{20} \text{ s}^{-1}$ $G_{H_2^+} \approx 1.44 \times 10^{22} \text{ s}^{-1}$	≈ 0.96 ≈ 2.5

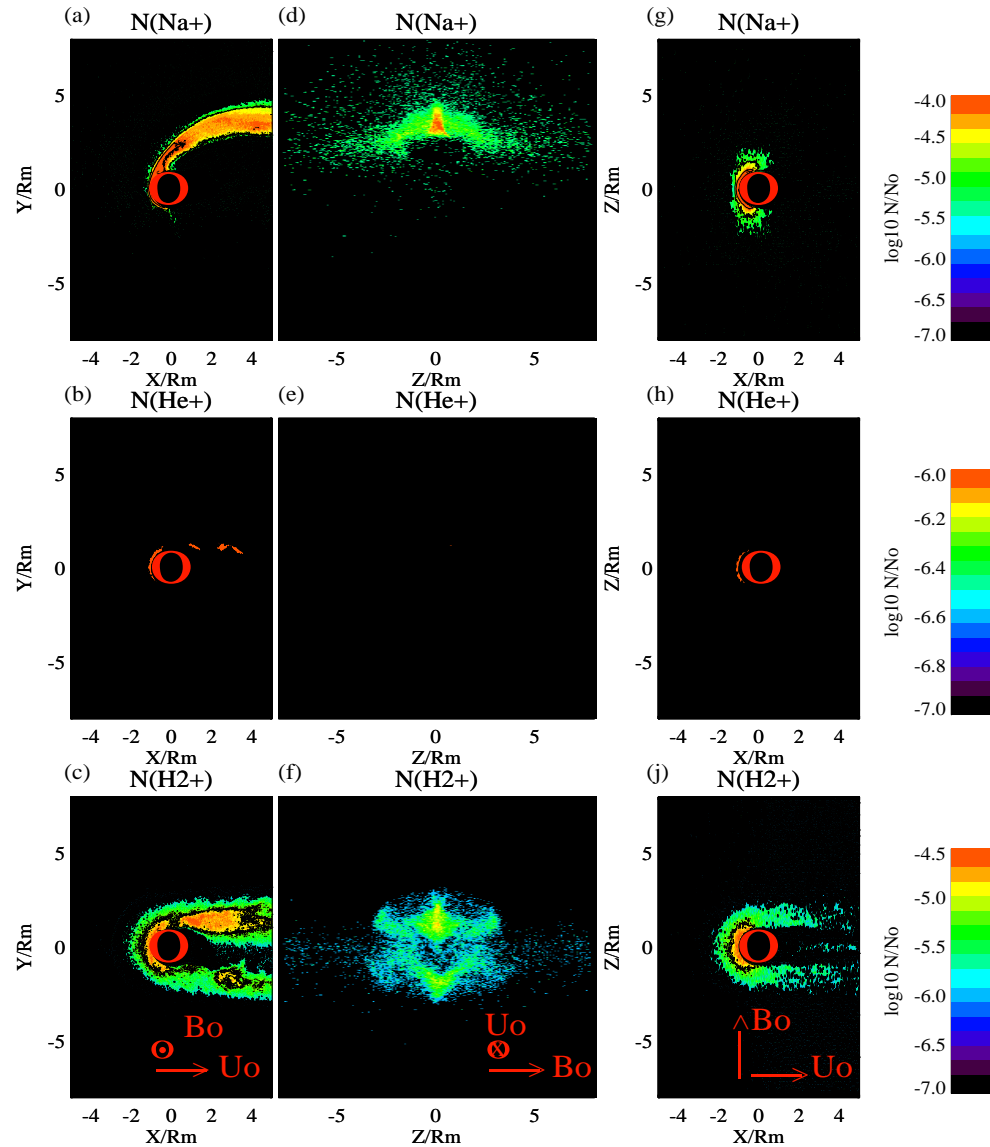
13. Plots of the SW extreme magnetic field, density, and moderate velocity (ARTEMIS).

Case 1. High SW density and magnetic field and moderate speed.



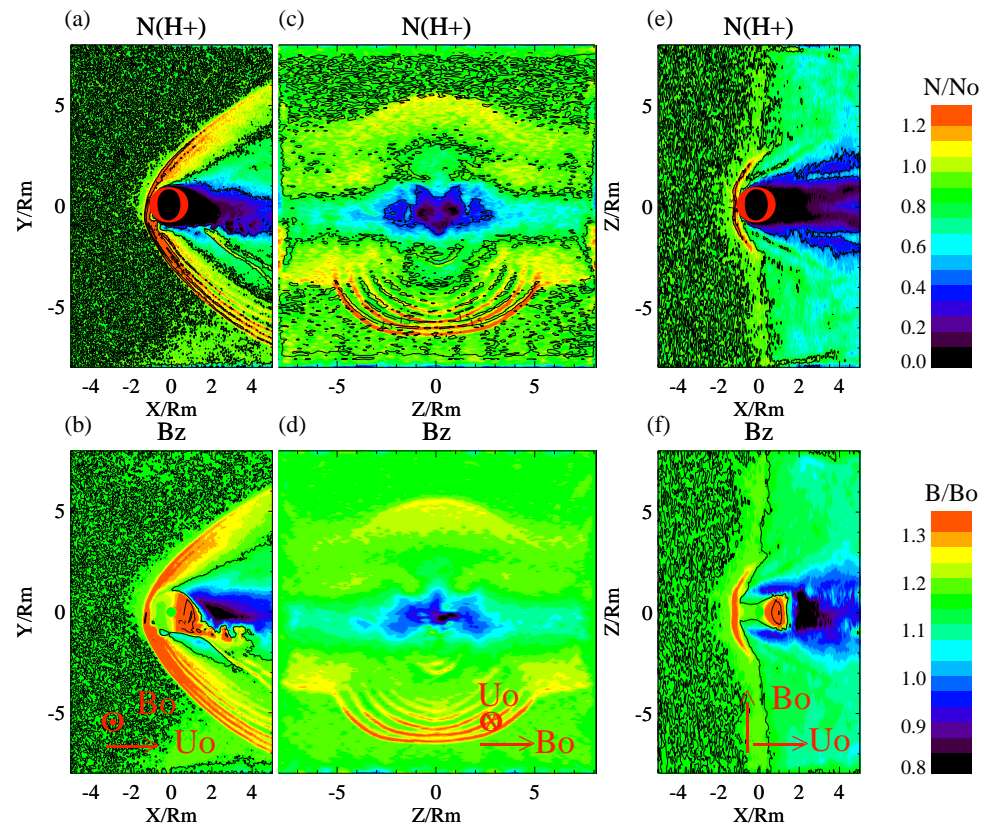
14. 2-D cuts of the pickup ion Na^+/H^+ density

Case 1. High SW density and magnetic field and moderate speed.
 $\theta_{UB} = 90^\circ$



15. 2-D cuts of background ions density and magnetic field

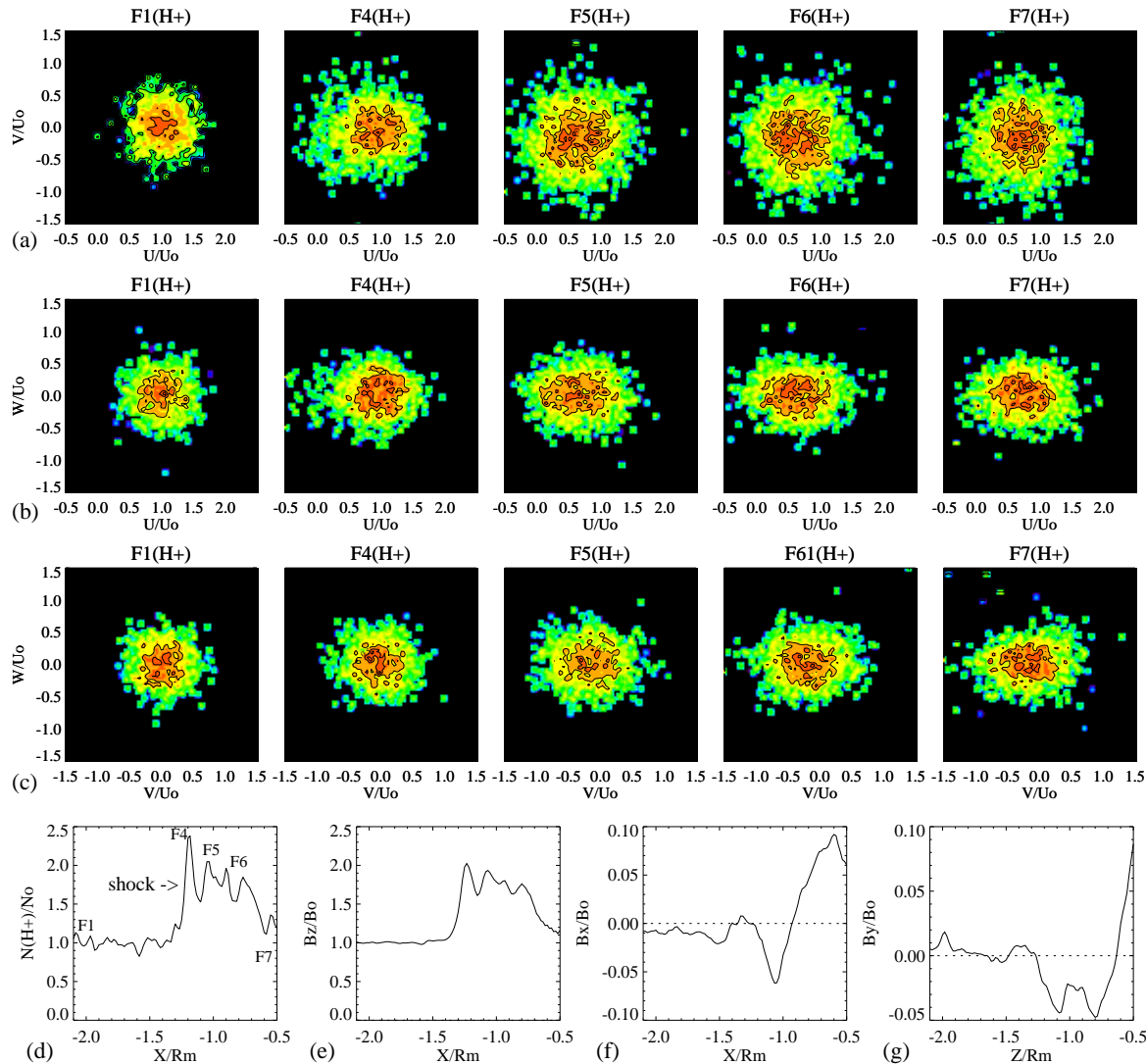
Case 1. High SW density and magnetic field and moderate speed.
 $\theta_{UB} = 90^\circ$



16. Non-Maxwellian velocity distribution functions (VDFs) for the

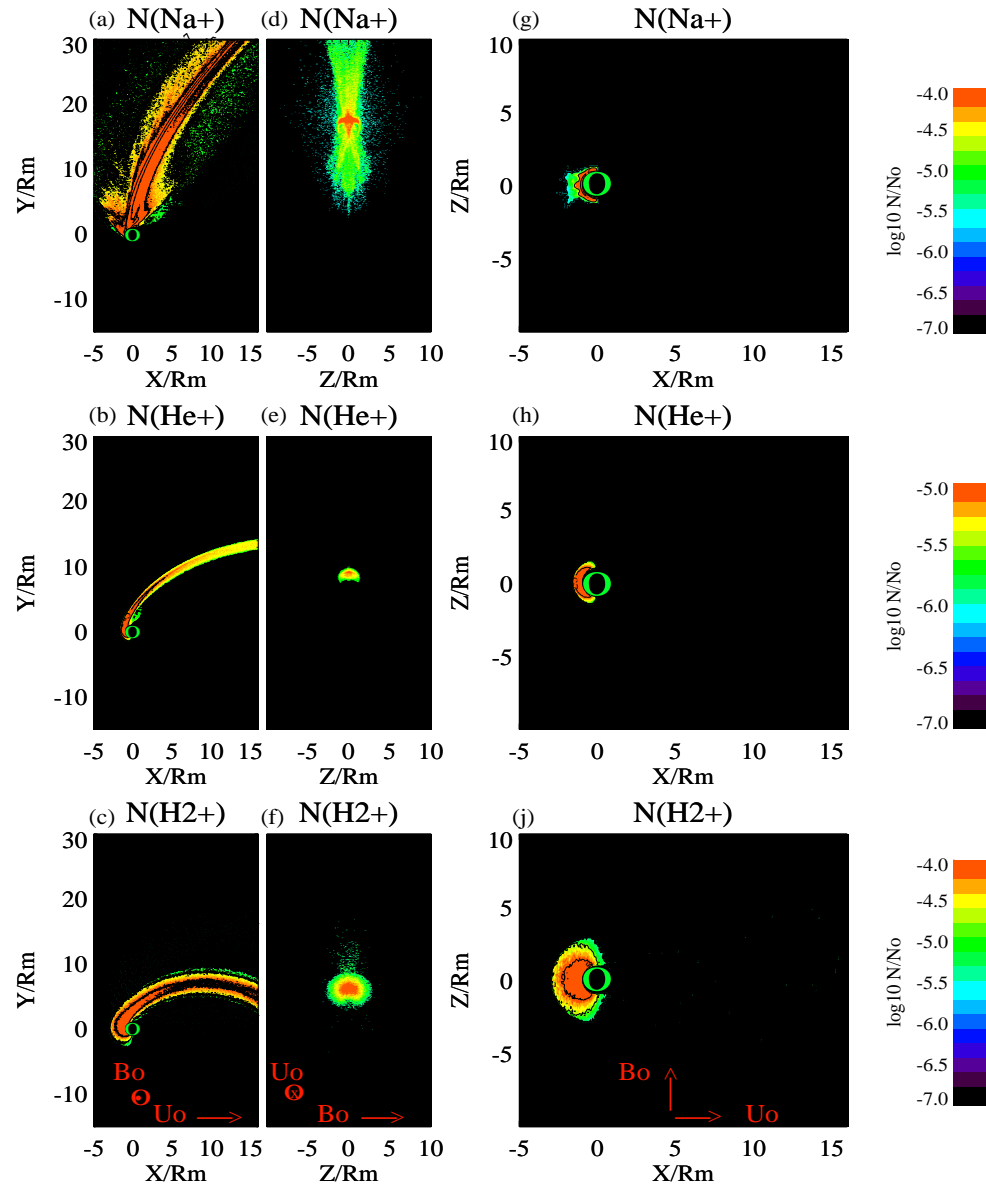
background (H^+) ions

Case 1. High SW density and magnetic field and moderate speed.
 $\theta_{UB} = 90^\circ$



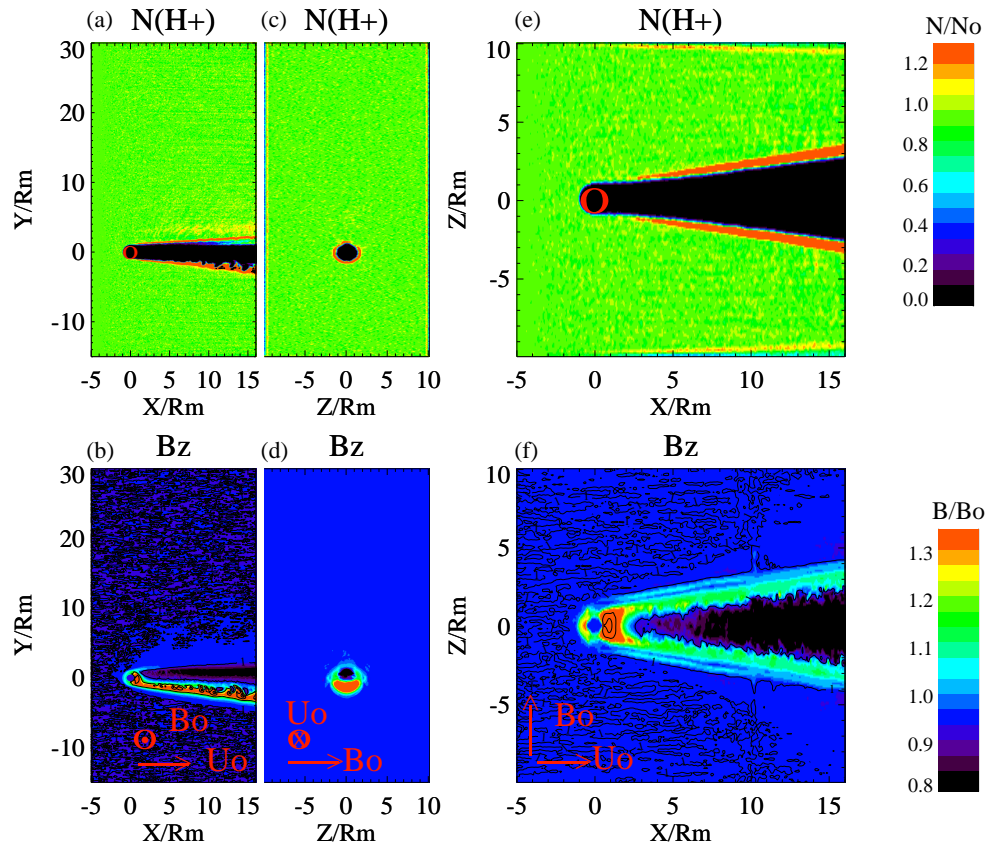
17. 2-D cuts of the pickup $N\alpha^+/H^+$ ion density

Case 4. High SW speed and moderate density, and magnetic field.
 $\theta_{UB} = 90^\circ$



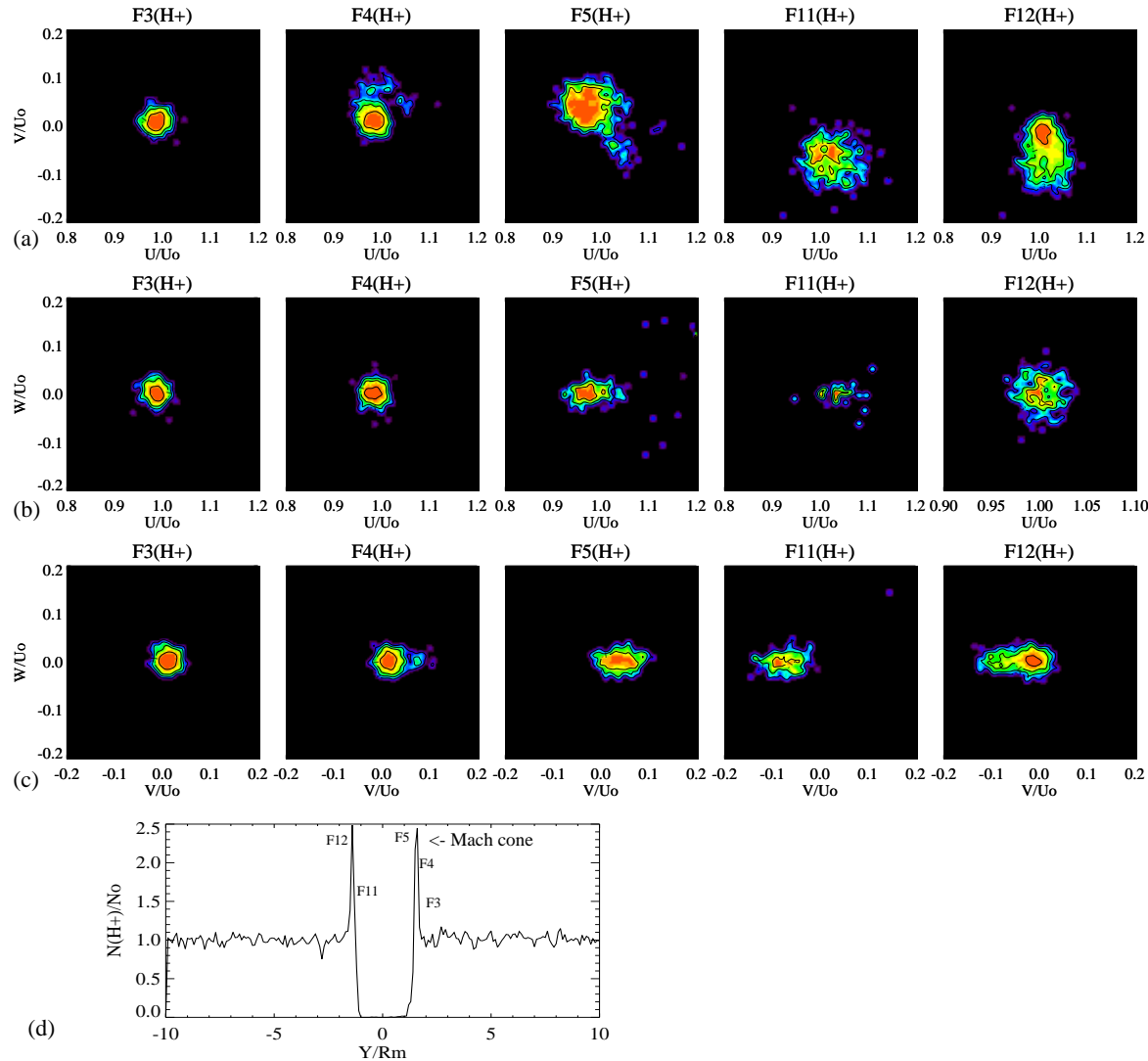
18. 2-D cuts of background ion density and magnetic field

Case 4. High SW speed and moderate density, and magnetic field.
 $\theta_{UB} = 90^\circ$



19. Non-Maxwellian velocity distribution functions (VDFs) for the background (H^+) ions

Case 4. High SW speed and moderate density, and magnetic field.
 $\theta_{UB} = 90^\circ$



20. Summary-1

A. Moon in the SW super-Alfvenic/sonic flow with extreme high density ($50 - 15$) cm^{-3} and magnetic field ($30 - 17$) nT (cases N.1 and N.2).

Quasi-perpendicular interaction:

- **The modeling shows a formation of a strongly asymmetrical bow shock-like wave and an asymmetrical plasma wake in the background plasma. This bow shock-like wave has an extended wing near the central 2-D cut across the incoming SW magnetic field and very short wing near the central 2-D cut which contains the incoming velocity and magnetic field line, unlike the standard bow shock near the planets e.g. Earth, Venus, Mars etc.**
- **A strong jump in ambient plasma density is about $\delta n \approx 2.4 n_0$ is observed at the front of the bow shock-like wave. The perturbations in the background plasma are found across the bow shock wave front.**

21. Summary-2

- **The non-Maxwellian background H^+ ion velocity distribution functions (VDFs) are found at the bow shock wave transition. The reflected/accelerated background ions are observed at the front of bow shock wave.**
- **The modeling with chosen parameters of the SW and ion production rate shows the cycloid-like motion (ion finite gyroradius effect) of the heavy Na^+ pickup ions with practically no interaction with lighter He^+ pickup ions and light H_2^+ pickup ions. The light pickup ion tails have an orientation along the incoming solar wind flow past the Moon because of their small gyroradius and drift in the electromagnetic field. The light H_2^+ pickup ions create split tail with a halo which is expanding along the magnetic field.**

22. Summary-3

B. Moon in the SW super-Alfvenic/sonic flow with extreme speed (≈ 1500 km/s) and moderate density and magnetic field:

- **The modeling shows a formation of the asymmetrical hypersonic Mach cone in the background plasma field with a jump in a density of about 2.5 across the Mach cone front.**
- **The heavy Na^+ ions form a complicated plasma tail. The core portion of the tail rotates in the SW electromagnetic field while the halo near the Moon has a strongly structured form. The modeling also shows a strong expansion of this tail. The light He^+ and H_2^+ pickup ions form tails which follow the cycloid trajectory but with a weak plasma expansion across this tail.**
- **The modeling shows non-Maxwellian VDF's for background ions near the Mach cone front. The background ions reflection was observed in the foot of the Mach cone, whereas a strong ion heating and phase-mixing were observed inside the ramp and downstream of the cone.**

23. Summary-4

The results of this work may be important for understanding the plasma processes in the plasma environment near very weak comets, asteroids, Pluto, and Europa.

Acknowledgment. This work was supported by NASA Grant (80NSSC20K0146) “Hybrid Fluid-Kinetic Model of the Processes in the Moon’s Plasma Environment” from Solar System Workings Program (NNH18ZDA001N-C.3 SSW2018). Computational resources were provided by the NASA High-End Supercomputing Facilities (Pleiades/Electra/Aitken-Ames, Discover-Goddard, Project HEC SMD 20-02357875).